On the existence of a local dipolar plasmon mode in doped small gold atomic arrays

J. Chen ⬤, L. Q. Lai, X. Yang, Q. H. Liu, and Y. B. Yu*

School of Physics and Electronics, Hunan University, Changsha 410082, China

Impurity doping in atomic chains provides a potentially effective way to adjust its electronic excitation. Recently, it was reported that doping transition-metal atoms into small gold atomic chains induces a local dipolar plasmon mode which corresponds to charge oscillations around the impurity atoms, whereas our studies indicate that such a local mode does not exist. In this paper, using time-dependent density functional theory, we extensively investigate the excitation properties of plasmons in doped gold nanostructures. Our results show that all the plasmon peaks are affected by impurity, and the corresponding plasmon modes mutate into different forms compared to pure gold atomic chains. The propagation of charge oscillations in some plasmon modes is blocked in the doped chain, so that the charges oscillate mainly in half of the chain. Furthermore, the 5*d* electrons of gold atoms reduce the energies and intensities of plasmon resonances for both the transverse and longitudinal modes, and cause the end and center features of the induced charge distributions to nearly vanish in the transverse plasmon modes.

I. INTRODUCTION

Metal atomic structures play an essential part in optoelectronics due to the unique properties of surface plasmon resonances such as local- and near-field enhancement, subwavelength binding of electromagnetic waves, and selective absorption of light [1–7]. The metal materials exhibit significant plasmon resonances in different scales. In terms of small clusters, Kummel *et al.* [8] have theoretically proved the existence of density oscillations even for the smallest metal clusters. Compared with large-scale structures, atomic structures with nanoscale dimensions make the quantum effect more obvious [9–12]. When the nanoparticles are subjected to an applied external electromagnetic field, free electrons on the surface of an atomic structure are polarized and produce a recovering force, which makes the free electrons oscillate periodically on the nanoparticle surface and results in an increase of electric field intensity. This phenomenon is called a "localized surface plasmon" (LSP) [13]. In addition, the resonance frequency of LSP is always related to impurities, atomic species, shapes, sizes, and the directions of the external field [14–26]. For example, Luther *et al.* [27] demonstrated that active on-chip control of localized surface plasmon resonances can be achieved by free-carrier doping of a semiconductor nanocrystal. Shu *et al.* [28,29] explained that the tunable plasmons can be implemented by changing the number of layers in N-doped graphene nanostructures. Meanwhile, Conley *et al.* [30] also have reported that arrays of mixed noble- and transition-metal chains might be used to manipulate the plasmon resonances, splitting them into several peaks and eventually achieving broadband photoabsorption. It is worth mentioning that the relativistic and spin-orbit effects have an important position in the plasmon resonances of noble

metals. Khodabandeh *et al.* [31] demonstrated that for Au atomic chains and rods doped by Ag atoms, the quantum effects, scalar-relativistic contributions, and spin-orbit coupling can significantly affect the oscillation strengths and energies of plasmon excitations. The influence of relativistic effects in Au chains is greater than that in Ag and Cu chains [32]. In addition, Gao *et al.* [33,34] introduced for the first time the end (TE) and the central (TC) modes in a pure Na chain, and then compared the differences and relations of K, Na, and Ag chains. The single-particle transitions and the quantum coherence of these transitions in the plasmon resonances are also investigated in longitudinal and transverse modes for Ag and Au nanowires [35–37]. With continual advances in nanotechnology, researchers can already use scanning tunneling microscopy or atomic force microscopy to observe and to manipulate a single atom, which allows us to place a dopant atom in an accurate position [38–41].

With respect to single-chain structures, the longitudinal plasmons in gold chains doped with a transition-metal atom (Ni, Rh, Fe) were comprehensively studied by Nayyar *et al.* [42], and due to the dopant an additional plasmon resonant peak appeared near the main peak in the optical absorption spectra. They ascribed the additional peak to the local plasmon mode which corresponds to charge oscillations around the impurity atoms, whereas they did not study the distributions of the induced charge. Motivated by their results and interpretations, we investigate the distributions of the induced charge at additional resonant peaks. Our results demonstrate that such local plasmon modes do not exist in doped gold atomic chains, and the impurity can only make the original spectra and induced charge distributions change markedly.

In this paper, we present detailed and systematic investigations for gold atomic structures containing an impurity, including a single atomic chain and a square array. We find that in the Au chain the oscillations of the charge density from

---

*apybyu@hnu.edu.cn

side to side are hindered by the dopant Ni on the longitudinal modes, and the oscillations of *s* electrons in half of the doped chain are suppressed on the transverse modes. Meanwhile, transverse plasmon resonances with weak features of TE and TC are disrupted by the effect of impurity. However, the local dipolar modes reported in Ref. [42] are not found in the doped Au chain. We also study the effects of 5*d* electrons on the plasmon resonance, and find that the energies and oscillation strengths of the plasmon resonance are considerably reduced by the screening of *d* electrons and *s-d* coupling for both the longitudinal and transverse modes, and the degree of *d*-electron obstruction on the transverse oscillations of 6*s* electrons is larger than that on the longitudinal oscillations. In addition, the results for doped square arrays show that local dipolar modes also do not appear in both the *s*- and *d*-electronic oscillating regions, while the whole charge oscillations in the two-dimensional (2D) modes are changed by the impurity. Meanwhile, we find the edge mode and the center mode when 5*d* valence electrons are not taken into account in pure gold square arrays.

II. COMPUTATIONAL METHODS

The electronic excitations of small metal chains and arrays are calculated using the time-dependent density functional theory (TDDFT) method. All these calculations are based on the real-time TDDFT (RT-TDDFT) code in the OCTOPUS package [43,44]. The local density approximation (LDA) [45,46] is used to describe the exchange-correlation potential. We have tried different functions of exchange correlations, and the results show that different exchange-correlation functions have little influence on the optical absorption spectra. Hartwigsen-Goedecker-Hutter pseudopotentials are used, and the pseudopotential can have a good effect instead of core electrons and the nuclei [47]. Also, the gold nanostructures are calculated taking $5d^{10}6s^1$ as valence electrons, unless otherwise specified. All the atoms are fixed in the Cartesian coordinates. The atomic chains are along the *x* axis, and the square arrays are perpendicular to the *z* axis. The impulse excitations are applied to the nanostructures in the longitudinal and transverse directions. In order to further illustrate the resonance mechanism of the plasmon modes, we calculate the induced charge distributions of the Fourier transform corresponding to each resonant peak. All the slices of the induced charge distributions are based on the method of MULTIWFN [48]. Here, we will compare the calculated results of the doped gold nanostructures with the pure ones.

The following is a brief description of the parameters used in our calculation. The simulation zone is defined by assigning spheres which surround each atom with a radius of 6 Å and a grid spacing is 0.25 Å. The atomic spacing of gold atoms is 2.89 Å, which is obtained by experimental measurements [49]. In the doped chains, the distance between Au and the transition-metal atoms is maintained at 2.36 Å, which is the same as Nayyar's parameter values. The distance becomes 2.89 Å in the arrays to retain the square shape. In real-time propagation, well-converged results are obtained after 15 000 time steps with a timescale of 0.003ℏ/eV and a momentum increase of 0.05 1/Å.
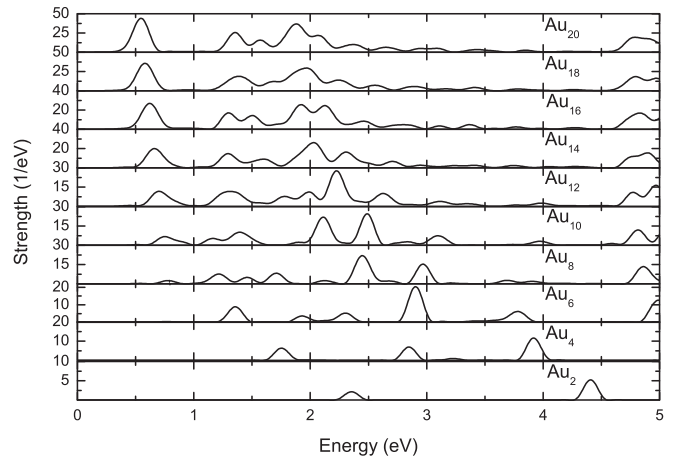

FIG. 1. The optical absorption spectra of linear gold chains, with a variable number of atoms from 2 to 20, to an impulse excitation applied in the longitudinal direction.

III. RESULTS AND DISCUSSIONS

A. Plasmon resonances in a one-dimensional chain structure

Figure 1 shows the optical absorption spectra of gold chains as a function of the length for longitudinal modes, which are consistent with the results obtained by Lian *et al.* [50] based on the linear response TDDFT (LR-TDDFT). For example, in the 20-atom gold chain (Au_{20}) the resonance energies 0.55 and 1.35 eV agree well with their results, and both the oscillation strengths are coincident quantitatively. However, our results are very different from the ones calculated by Nayyar *et al.* using the LR-TDDFT method [42]. One can see that in our results, the resonance energies of the peaks are smaller than the values of Nayyar's results, and most of the resonant peaks with moderate optical strengths are distributed in the region from 1 to 3 eV.

In the following, we will study the effects of impurities on the plasmon excitations for doped gold chains. Nayyar *et al.* [42] reported an additional plasmon peak in the optical absorption spectrum of an Au chain doped with Ni, and interpreted it as the local plasmon mode around the site of the dopant Ni atom. Meanwhile, Li *et al.* [51] also employed the same method to calculate the Ag chains doped with transition-metal atoms (Fe, Cu, Ni, Rh), and reached the same conclusions. However, the two groups did not present the distributions of the induced dynamic charge that correspond to the additional plasmon peaks. In order to verify their results and conclusions, we recalculate the spectrum of the doped chain $Au_{19}Ni_1$-10, and the results are shown in Fig. 2. The absorption spectrum of the chain $Au_{19}Ni_1$-10 is quite different from that of the chain Au_{20}, especially in the visible light range (1.61–3.10 eV). The plasmon peaks of the doped chain become more complex, and the main peak at 0.64 eV has a blueshift. On the other hand, we find that some additional plasmon peaks appear in the doped chain, e.g., the peak at 1.22 eV in the doped chain $Au_{19}Ni_1$-10 which is an Au_{20} chain doped with a Ni atom at site 10, and we call them "the impurity peaks," whereas, contrary to what was reported by Nayyar *et al.*, we do not find a significant impurity peak near
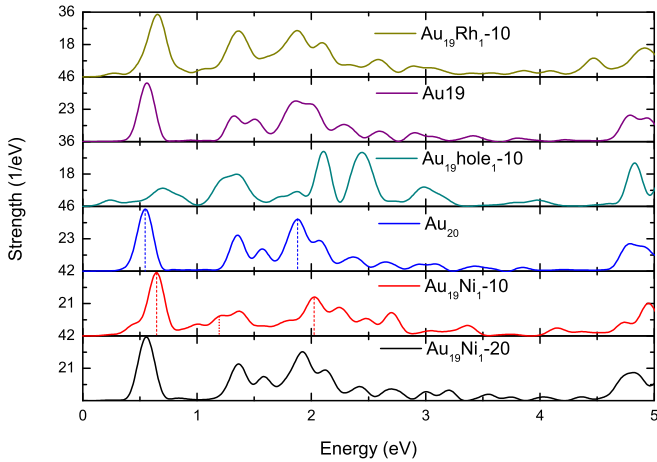
FIG. 2. The optical absorption spectra of different atomic chains, with the impurity atom at the middle (at site 10) or the edge position (at site 20), to an impulse excitation applied in the x direction.

FIG. 3. The induced charge distributions of the Fourier transform are in the planes $z = 0$ Å, which correspond to the resonance energies of the gold chain Au_{20}, (a) 0.55 eV and (b) 1.88 eV, and the resonance energies of the doped chain $Au_{19}Ni_1$-10, (c) 0.64 eV, (d) 1.22 eV, and (e) 2.03 eV, respectively. The impulse excitations are added in the x direction.

the main peak. When the dopant Ni is replaced by a Rh atom, the main peak of the doped chain $Au_{19}Rh_1$-10 at 0.65 eV has a displacement in a similar way as in the chain $Au_{19}Ni_1$-10, and an unobvious additional peak appears in the point of 1.09 eV. On the other hand, the absorption spectrum of the chain with a hole at site 10 is similar to the spectrum of Au_{10}, which has two plasmon peaks at 2.11 and 2.44 eV. This result can be understood as a superposition of two spectra of Au_9 and Au_{10}. In addition, when the dopant Ni is at site 20, one can find that the shape of the spectrum is very similar to that of the pure gold chain Au_{20}, and the spectrum has only a small blueshift. We speculate that the dopant in the end of the doped chain has less effect on the longitudinal mode.

To further illustrate the conclusion mentioned above, we calculate the Fourier transforms of the induced charge distributions that correspond to those plasmon peaks, where the formula of the Fourier transform is $\delta\rho(\vec{r}, \omega) = \int_0^T \exp(i\omega t)(-e)[\rho(\vec{r}, t) - \rho(\vec{r}, 0)]dt$. Here, T is the total evolution time of the electron wave functions, and $\rho(\vec{r}, t)$ represents electron densities at position $\vec{r}$ and time t. It is worth pointing out that only the imaginary part of the Fourier transforms of the induced charge distributions would be presented because it corresponds to the optical absorption. The resonance energies of the gold chain Au_{20} are 0.55, 1.35, 1.57, 1.88, 2.07, 2.37, 2.65, 2.95, 3.08, 3.43, 3.85, and 4.79 eV, while the resonance energies of the doped chain $Au_{19}Ni_1$-10 are 0.64, 1.01, 1.22, 1.37, 2.03, 2.24, 2.48, 2.70, 3.04, 3.37, 3.74, 4.15, 4.74, and 4.95 eV. After the calculations of all the induced charge distributions at those resonance energies, we do not find any mode of particular concern, especially any local plasmon mode as described in Ref. [42]. Here, we choose some representative charge distributions to show the difference between the pure gold chains and the doped gold chains. Figure 3 shows the induced charge distributions of the main peaks for longitudinal resonances in the doped chain $Au_{19}Ni_1$-10 and in the pure gold chain Au_{20}, where the induced charges are in the plane $z = 0$ Å. The induced charges at the main peak in the inner and outer region of each atom have opposite signs for the pure chain Au_{20}, as shown in Fig. 3(a),
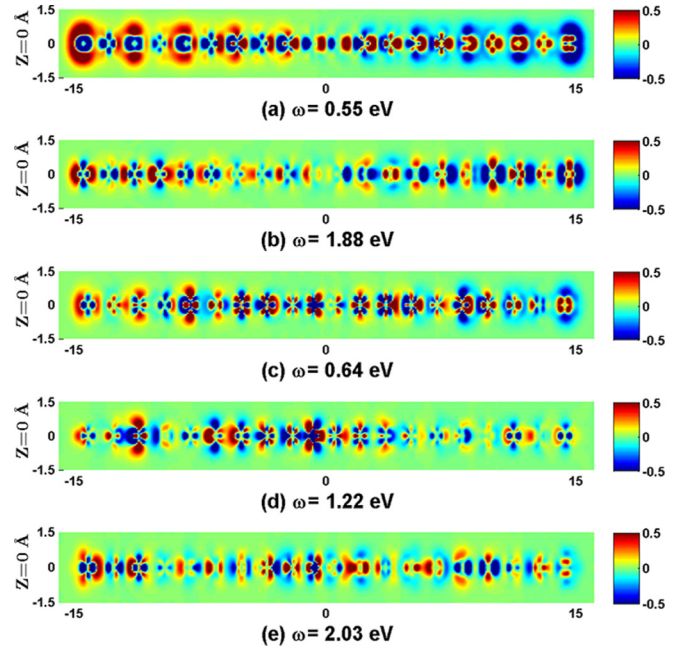
which means that the oscillations of the induced charges in the inner and outer regions of the atoms are opposite in phase. Figure 3(c) shows the induced charge distribution at the main resonant peak of the doped chain $Au_{19}Ni_1$-10, and in comparison with Fig. 3(a) we find that the oscillating charges are to some extent suppressed by the dopant, but the charges in the vicinity of the impurity are significantly enhanced. Figure 3(d) shows that at a resonance energy 1.22 eV the dopant Ni seems to block the oscillation of the induced charge from one side to another, and local polarizations appear in the chain, which weaken the total polarization. The distribution of induced charges at 2.03 eV shown in Fig. 3(e) is remarkably changed by the Ni atom in comparison with Fig. 3(b), and also the charges in the vicinity of the impurity are significantly enhanced. In addition, in Figs. 3(b) and 3(e) one can find that the induced charges distributed in the inner region occupy a dominant position. By comparing various induced charges under different conditions, we conclude that the impurity atoms can lead to additional plasmon resonances, and give rise to charge redistributions in the doped metal atomic chains; however, for all the doped chains, in the distributions of an induced oscillating charges we cannot find a local mode of distribution in which the charges oscillate only around the impurity as is described in Ref. [42]. By the way, with different kinds of general gradient approximations (GGA), such as GGA-PW91 [52,53], GGA-PBE [54], GGA-AM05 [55,56], and hybrid GGA-B3PW91 [57], and the random phase approximation, we also calculate the absorption spectra and the corresponding induced charge distribution for all the observable resonant peaks, and find that the obtained results are in agreement with each other. Therefore, we believe that
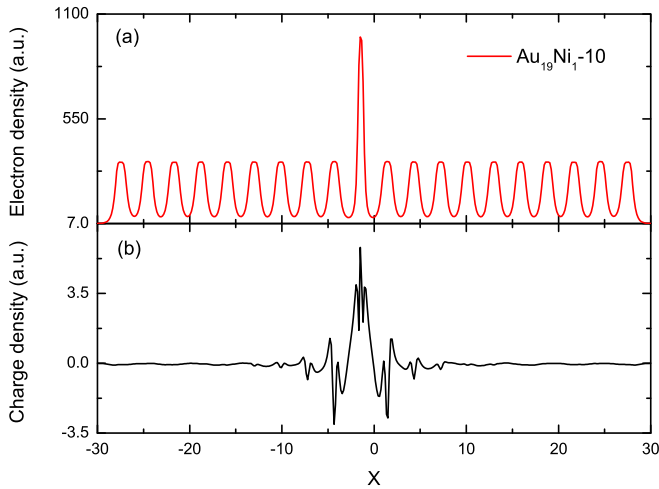
FIG. 4. The electron density of the ground state as a function of x corresponding to the doped chain $Au_{19}Ni_1$-10 in (a). The charge density $-e(\rho - \rho_0)$ as a function of x shows that the electron density ρ subtracts the "chain $Au_{19}Ni_1$-10 without impurity scattering," $\rho_0 = \rho_{Au_{20}} + \rho_{Ni} - \rho_{Au}$, in (b).

no local mode of a plasmon, in which the induced charges oscillate around the impurity, appears in the small atomic chains, at least in the dipolar response case.

We now calculate the electron density of the ground state as a function of x in the doped chain $Au_{19}Ni_1$-10, and the result is shown in Fig. 4(a). In order to reveal the Friedel oscillation obviously, in Fig. 4(b) we plot the charge density $-e(\rho - \rho_0)$ as a function of x. Here, ρ is the electron density of the ground state in the doped chain $Au_{19}Ni_1$-10, and $\rho_0 = \rho_{Au_{20}} + \rho_{Ni} - \rho_{Au}$ is the electron density of the "chain $Au_{19}Ni_1$-10 without impurity scattering," where $\rho_{Au_{20}}$ is the electron density in the pure chain Au_{20}, and ρ_{Ni} and ρ_{Au} are the electron densities of one Ni and one Au atom doped at site 10, respectively. The definition of charge density in this way is because the Ni atom has more valence electrons than the Au atom in the calculation. Figure 4(b) displays the feature of charge density induced by the impurity atom Ni. The Friedel oscillation only extends to the region with a radius of 2–3 atoms, which can be also seen in the Mulliken charge distribution presented in Ref. [42]. However, the local impurity charges do not give rise to local plasmons. This seems to us that the Friedel oscillation, which is the static charge fluctuation induced by an impurity in the ground state, has little relation to the plasmon of dynamic charges.

Next, we investigate the transverse plasmon modes of the chain structures by applying an impulse excitation in the y direction. Figure 5 shows the optical absorption spectra of pure gold chains as a function of the length. It is not difficult to find that the resonance energies of the plasmon peaks in all pure gold chains are larger than 5 eV. The plasmon peaks slightly shift toward blue with an increase of the chain length. It can be understood that the transverse resonances are mainly related to the interband excitation between the occupied and unoccupied bands. The electron transition motivated by the impulse excitation mainly occurs near the Fermi level, which is less affected by the coupling of neighboring atomic orbitals. On the other hand, the requirements of energies in the inter-
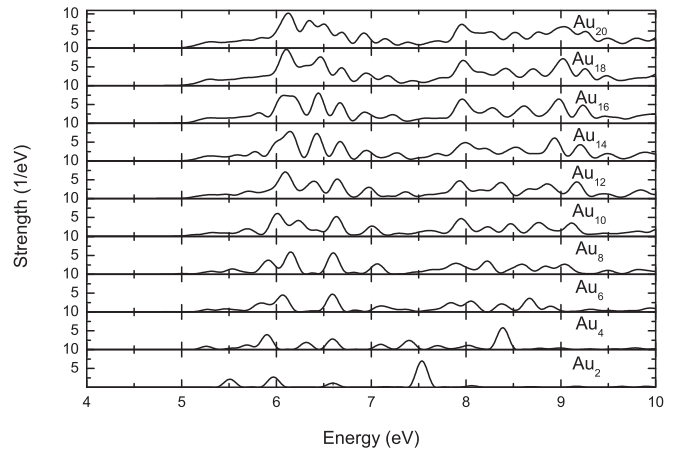

FIG. 5. The optical absorption spectra corresponding to linear gold chains, to an impulse excitation applied in the y direction, with a variable number of atoms from 2 to 20.

band transition are greater than that in the intraband transition, hence the low-limit resonance energy on the transverse modes is larger.

In order to understand the effect of impurities on transverse modes, we compare the optical absorption spectra in the y direction of doped chains with the ones of pure gold chains, as shown in Fig. 6. One can find that the spectrum of $Au_{19}hole_1$-10 is similar to that of Au_{20}, and the spectrum of $Au_{19}Ni_1$-10 is similar to that of $Au_{19}Ni_1$-20, but somewhat different from that of Au_{20}. These results suggest that the impurity position has little effect on the optical absorption spectra in the transverse direction. This may be because the transverse modes are mainly caused by the interband transition, which is only slightly influenced by the effect of the dopant. Comparing the spectrum of chain $Au_{19}Ni_1$-10 with Au_{20}, one can find that the three main peaks of Au_{20} around 6.31 eV merge to one peak of $Au_{19}Ni_1$-10, which is very different from the longitudinal case.
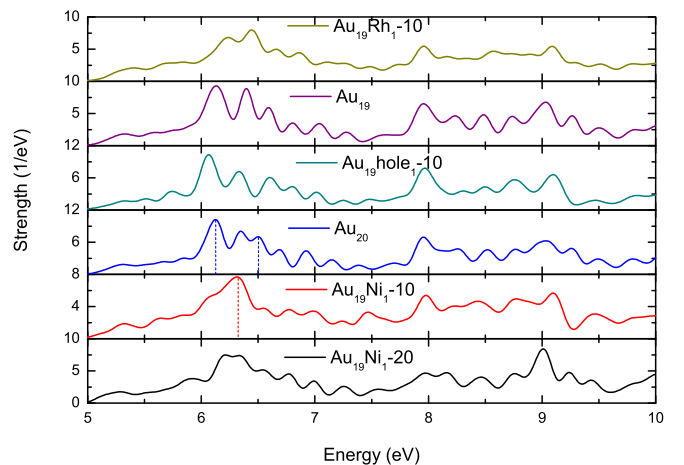

FIG. 6. The optical absorption spectra of doped gold chains and pure gold chains, to an impulse excitation applied in the y direction, with the impurity atoms including Ni, Rh, and a hole.
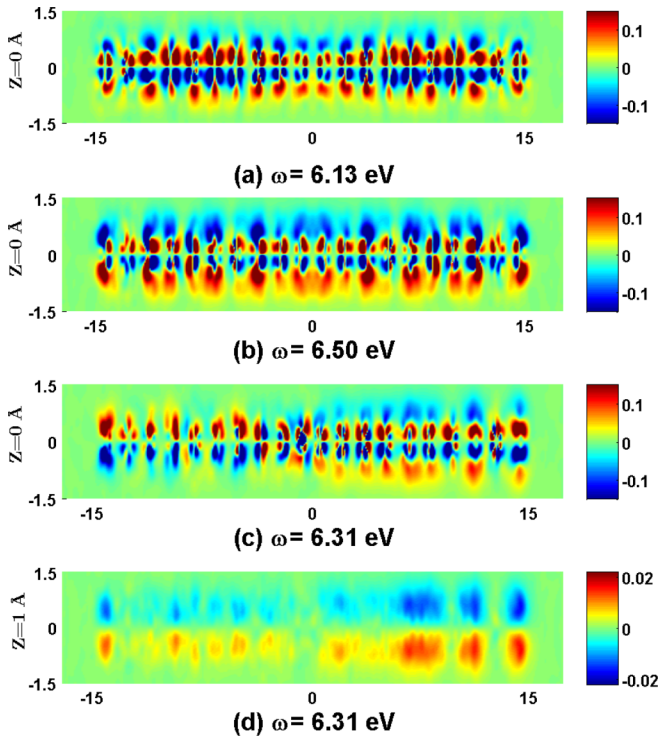
FIG. 7. The induced charge distributions of the Fourier transform of the transverse plasmon are in the planes $z = 0$ Å and $z = 1$ Å, which correspond to the resonance energies of the pure chain Au_{20}, (a) 6.13 eV and (b) 6.50 eV, and the resonance energies of the doped chain $Au_{19}Ni_1$-10, (c) 6.31 eV and (d) 6.31 eV, respectively.
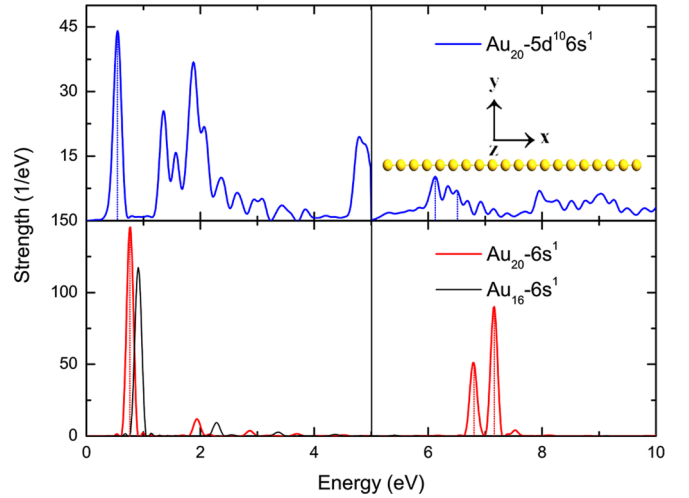

FIG. 8. The optical absorption spectra of Au_{16} and Au_{20} without the $5d$ valence electrons (bottom panel), and the one of Au_{20} with $5d$ valence electrons (top panel). The impulse excitations are applied in the longitudinal (left) and transverse directions (right), respectively.

To elucidate the mechanism of these transverse plasmon resonances, we now study the induced charge distributions of the transverse plasmons. In Figs. 5 and 6, one can find many resonant peaks, which correspond to the resonance energies of the gold chain Au_{20}, 6.13, 6.35, 6.50, 6.69, 6.92, 7.15, 7.39, 7.70, 7.96, 8.26, 8.52, 8.77, 9.03, 9.26, 9.49, and 9.80 eV, and the resonance energies of the doped chain $Au_{19}Ni_1$-10, 6.31, 6.55, 6.77, 6.99, 7.24, 7.47, 7.98, 8.23, 8.43, 8.77, 9.10, and 9.46 eV. Similar to the discussion about longitudinal resonances, we choose some representative charge distributions to show the difference between the pure gold chain and doped chain in Fig. 7. Here, Figs. 7(a) and 7(b) show the charge distributions at the two main resonant peaks of the pure gold chain Au_{20}, which somewhat display the features of TE and TC modes [33,34]. The oscillation strengths of plasmon resonances in both sides of the chain are stronger than that in the middle in Fig. 7(a), while the strength of the plasmon resonance in Fig. 7(b) is opposite to it. One can find that the characters of TE and TC modes are not obvious, and below we will illustrate that the phenomenon is due to the effect of $5d$ electrons . Figures 7(c) and 7(d) show the charge distributions in the planes $z = 0$ Å and $z = 1$ Å for the main peak of 6.31 eV in the doped chain $Au_{19}Ni_1$-10, which is between the two peaks of 6.13 and 6.50 eV in the Au_{20} chain, and can be regarded as a merging of the two transverse modes into one mode due to the dopant Ni. One can find that Fig. 7(c) exhibits a more complex structure than Figs. 7(a) and 7(b), and in the plane $z = 0$ Å the polarization

of the charges on the left seems to be opposite to the right, while in the plane of $z = 1$ Å they are the same. Meanwhile, the oscillation strength of the induced charge on the left is much weaker than on the right. This indicates that the dopant weakens the oscillation of induced charge on the left. Since d electrons are relatively closer to the nucleus of Au atoms than s electrons, we infer that the charge oscillations in the outer shell are dominated by $6s$ electrons, and the ones in the inner shell are dominated by $5d$ electrons. Based on these two points, we conclude that the impurity disrupts the original two transverse plasmon resonances mainly by suppressing the oscillation of s electrons in half of the doped chain.

In order to further understand the effect of $5d$ electrons on the plasmon resonances, we calculate the optical absorption spectrum of the Au_{20} chain only taking $6s^1$ as the valence electrons. In this case not only is the effect of d-electron screening [58] to the $6s$ electrons ignored, but also the s-d hybridization [59] is not considered. The optical absorption spectra are clear the resonant peaks are the same as the ones found by Liu and Zhang using the RT-TDDFT method [60]. In addition, Wang and Ke [61] reported the TE and TC modes of transverse excitation plasmons in Au chain doped with two Ni atoms. However, we calculate the optical absorption spectra of chain $Au_{16}Ni_{2(9)}$ without $5d$ valence electrons, which are in good agreement with their result, where $Au_{16}Ni_{2(9)}$ is the chain Au_{18} doped with two Ni atoms at sites 9 and 10. Therefore, the studied chains in Ref. [61] are in fact the ones without $5d$ valence electrons. As a concrete example, the spectra of the Au_{20} chain are shown in Fig. 8, where the main resonant peak (at 0.55 eV) of the chain with $5d$ valence electrons has a redshift compared with that (at 0.76 eV) of the chain without $5d$ valence electrons. The observed redshift of the plasmon peaks can be qualitatively explained in terms of the s-d screening interaction, and the s-d and p-d hybridizations in the collective excitations. The screening of d electrons causes an overall lowering of resonance energy of the spectra as pointed by Liebsch [62], and the s-d and p-d hybridizations diminish
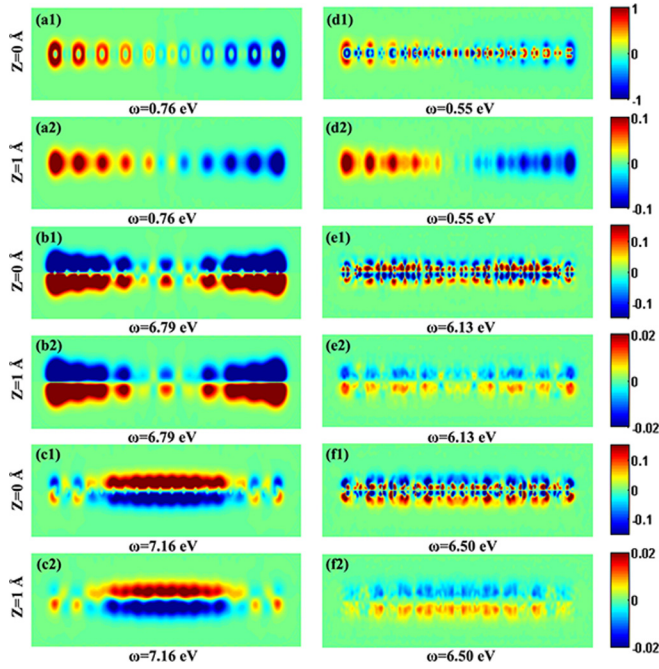
FIG. 9. The induced charge distributions of the Fourier transform of pure chain Au_{20} are in the planes $z = 0$ Å and $z = 1$ Å. (a) and (d) are longitudinal charge oscillations at resonance energies 0.76 and 0.55 eV, respectively. (b), (c), (e), and (f) are the transverse charge oscillations at resonance energies 6.79, 7.16, 6.13, and 6.50 eV, respectively. $5d$ valence electrons are not taken into account in the figures of the left column, while they are considered in the other figures of the right column.

the energy-level interval. On the other hand, in the chain with $5d$ valence electrons the oscillation strength of the spectrum is significantly reduced, which may be because the electron mobility is reduced by the s-d coupling. This is shown clearly in Fig. 9, which are the induced charge distributions in atomic planes $z = 0$ Å and $z = 1$ Å, respectively. Figure 9(d1) indicates that in the chain with $5d$ valence electrons the longitudinal oscillation has a phase difference of π between the inner and outer space of the atoms. Since $5d$ valence electrons are mainly localized in the inner shell of atoms, this phase difference illustrates the electric screening between the charges of s and d electrons, and hence the oscillation of s-electron charges is suppressed. A similar case can be seen in the transverse oscillation [Figs. 9(e) and 9(f)]. By comparing Figs. 9(b2) and 9(e2), we find that the oscillation strength of $6s$ electrons without the effect of $5d$ valence electrons is much stronger than the one with the effect of $5d$ valence electrons, while the oscillation strength of the induced charge in Fig. 9(a2) is only slightly stronger than Fig. 9(d2). We can conclude that the degree of d-electron obstruction on the transverse oscillations of $6s$ electrons is more considerable than on the longitudinal oscillations. It is worth mentioning that we have used real-time propagation along with scalar-relativistic pseudopotentials to calculate the absorption spectra, as done by Yan *et al.* [34]. In Fig. 8, the longitudinal optical absorption spectrum of Au_{16} without $5d$ valence electrons is quite close to the results at the nonrelativistic level reported by Khodabandeh *et al.* [31], but has a somewhat blueshift
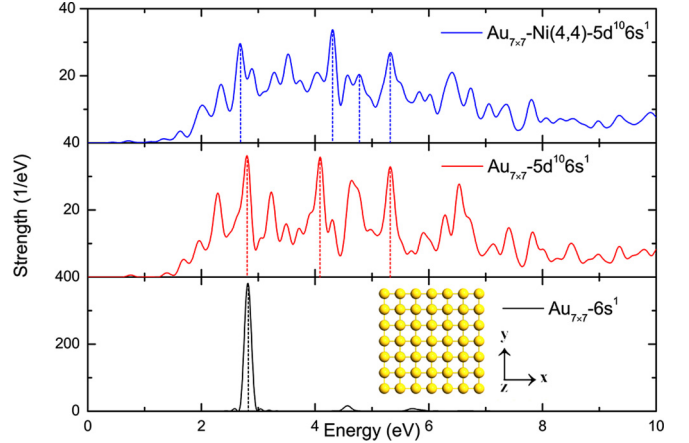

FIG. 10. The optical absorption spectrum of doped gold array $Au_{7\times7}$-Ni(4,4) including a dopant Ni at site (4,4), by comparing with the spectrum of pure gold array $Au_{7\times7}$. The figure in the last row does not take into account $5d$ valence electrons. The direction of an impulse excitation is parallel to the plane along the x axis.

relative to the latter; the blueshift becomes larger, and the strength is suppressed in comparison with the results at the scalar-relativistic and fully relativistic levels. This indicates that the influence of d electrons on the plasmon spectrum would be enhanced by considering the relativistic effect, as shown in Ref. [31] that the d electrons and relativistic effects have the same influence on the strength and energy of plasmon resonance.

B. Plasmon resonances in a two-dimensional array structure

Similarly, we investigate the plasmon excitations in square arrays. Figure 10 shows the optical absorption spectrum of the 2D doped gold array $Au_{7\times7}$-Ni(4,4) compared with the 2D pure gold array $Au_{7\times7}$. Here, the impulse excitation is applied in the x direction. The resonance energies of the square atomic array $Au_{7\times7}$ are 2.29, 2.80, 3.23, 3.49, 3.72, 4.09, 4.30, 4.64, 4.98, 5.32, 5.69, 5.91, 6.29, and 6.53 eV, while the resonance energies in the doped array $Au_{7\times7}$-Ni(4,4) are 2.20, 2.35, 2.68, 2.89, 3.28, 3.53, 3.73, 4.03, 4.31, 4.57, 4.78, 5.32, 5.83, 6.02, 6.41, and 6.74 eV, respectively. Because there are many plasmon peaks with roughly equivalent strengths in the optical absorption spectra, we only discuss those peaks having obvious oscillation strengths. The strengths of the three peaks (i.e., 2.68, 4.31, and 5.32 eV) in the doped square array are smaller than those in the pure square array (i.e., 2.80, 4.09, and 5.32 eV). Also, with the effect of the dopant Ni, the peak in the pure square array with a spread around 4.64 eV splits into two peaks at 4.57 and 4.78 eV. We can observe that the peaks become unsharp, and the number of plasmon peaks increases due to the effect of the impurity. The results show that the impurity changes the whole spectra of 2D arrays. In order to study the effect of d electrons, we also present the optical absorption spectrum of the pure gold array $Au_{7\times7}$ without $5d$ valence electrons in the bottom panel. The structure of this spectrum is simple and clear, and has only one large main peak at 2.82 eV. This illustrates the significant effect of $5d$ valence electrons on the plasmon excitations in the square
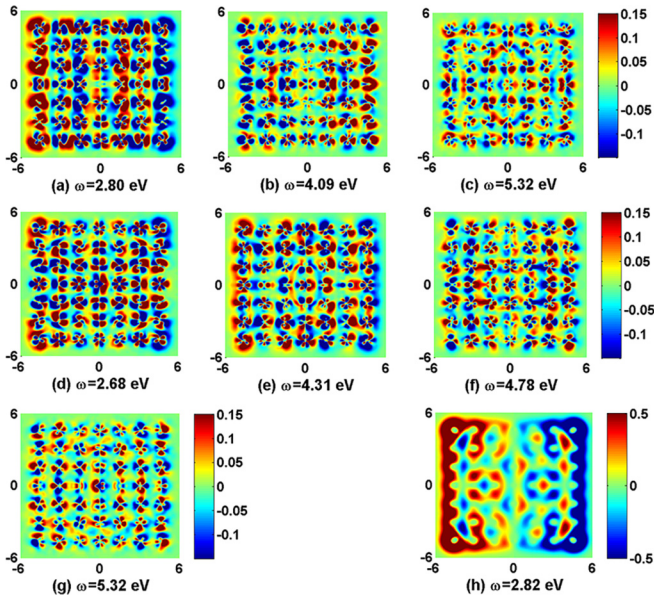
FIG. 11. The induced charge distributions of the Fourier transform in the plane $z = 0$ Å corresponding to the longitudinal plasmon. The resonance energies of the pure gold array $Au_{7\times7}$ are (a) 2.80 eV, (b) 4.09 eV, and (c) 5.32 eV. The resonance energies of the doped gold array $Au_{7\times7}$-Ni(4,4) are (d) 2.68 eV, (e) 4.31 eV, (f) 4.78 eV, and (g) 5.32 eV, respectively. Without the effect of d electrons, the induced charge distributions of resonance energy 2.82 eV are shown in (h).

FIG. 12. The optical absorption spectrum of the doped square array $Au_{7\times7}$-Ni(4,4) including the dopant Ni at site (4,4), by comparing with the one of the pure square array $Au_{7\times7}$. The figure in the last row does not take into account $5d$ valence electrons. The impulse excitation is perpendicular to the square arrays along the z axis.

array. Recently, Xue *et al.* [26] reported studies of plasmon excitations in square atomic arrays by using a free-electron gas model, in which the excitation field is a point-charge field instead of an optical field, and in their results an absorption spectrum for the half filling of electrons is similar to the above result for the square without d valence electrons.

Figure 11 shows the induced charge distributions for the longitudinal resonances in the square arrays. All the induced charge distributions in the array display a similar pattern, and we only show the results of the main peaks, the subpeaks, and the additional peaks. The induced charge distributions in the pure gold array for resonance energies 2.80, 4.09, and 5.32 eV are shown in Figs. 11(a)–11(c), respectively. In the doped square array, the resonance energies are 2.68, 4.31, 4.78, and 5.32 eV, and the corresponding induced charges are shown in Figs. 11(d)–11(g). In the doped array the induced charges around the dopant Ni at a peak of 2.68 eV have a larger oscillation strength than the charges at the same position and a corresponding peak (at 2.80 eV) in the pure gold array, while the induced charge distributions of the two additional peaks (at 4.31 and 4.78 eV) are not found to have obviously different characteristics. These results show that the impurity changes the whole distributions of induced charge in the square arrays, especially in the vicinity of the impurity, as was pointed out in Ref. [21]. Meanwhile, here we also do not find a local mode of the plasmon in which the induced charges oscillating around dopant Ni appear in the 2D arrays. Figure 11(h) shows the induced charge distribution at the peak of 2.82 eV in the pure gold square array without $5d$ valence electrons. The charge oscillation is antisymmetric with respect to the center
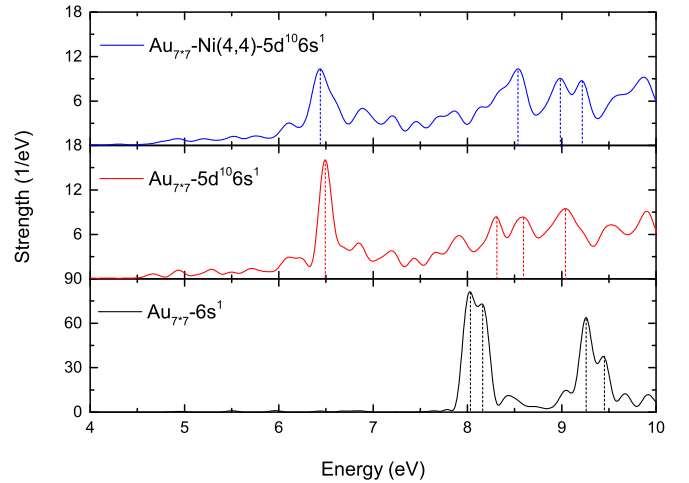
line perpendicular to the direction of the impulse excitations, and its amplitude reaches the maximum on the ends of the array. This result is considerably different from the atomic array with $5d$ valence electrons [Fig. 11(a)], and is somewhat similar to the one reported by Wang *et al.* [17] for Na atomic arrays, in which the induced charge is mainly distributed around the four corners of the arrays. In a comparison of an array with $5d$ valence electrons to one without $5d$ electrons, the effect of d electrons makes the induced charge distribution more complex.

Next, we study the out-of-plane plasmon mode by calculating the optical absorption spectra under an impulse excitation in the direction perpendicular to the 2D atomic arrays. Figure 12 shows a comparison of the optical absorption spectrum of the doped square array $Au_{7\times7}$-Ni(4,4) with a pure square array $Au_{7\times7}$. The resonance energies of the pure square array $Au_{7\times7}$ are 6.11, 6.22, 6.49, 6.85, 7.20, 7.44, 7.67, 7.91, 8.30, 8.59, 9.04, 9.53, and 9.90 eV, while the resonance energies of the doped square array $Au_{7\times7}$-Ni(4,4) are 6.11, 6.44, 6.89, 7.20, 7.46, 7.71, 7.86, 8.16, 8.54, 8.98, 9.23, 9.62, and 9.87 eV, respectively. It can be easily seen that the absorption onset is roughly 4.5 eV, somewhat lower than that of the one-dimensional (1D) situations. This may be because the band gap of 2D systems is smaller than the 1D band gap. Meanwhile, the impurity causes the intensity of the main peak to decrease, and some of the secondary peaks split in two or merge, but the overall spectrum changes little. In addition, for the pure square array $Au_{7\times7}$ without $5d$ valence electrons (see the bottom panel of Fig. 12) the absorption spectrum of a transverse excitation is above 7.5 eV, and the resonance energies are 8.03, 8.15, 8.43, 9.05, 9.26, 9.44, 9.67, and 9.92 eV. We can extrapolate that the degree of the redshift caused by the effect of $5d$ valence electrons in 2D systems is greater than the 1D case.

The induced charge distributions of the transverse-mode plasmons in 2D arrays are presented in Fig. 13. As mentioned above, $5d$ electrons make a prominent contribution to the
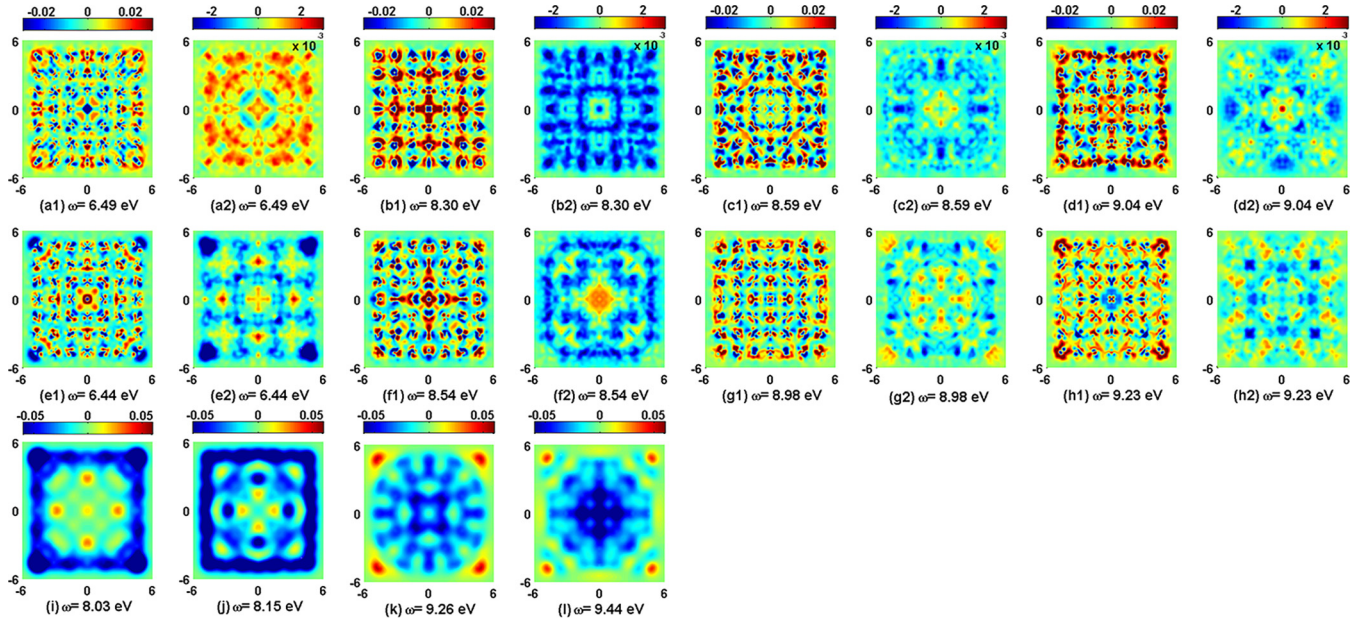
FIG. 13. The induced charge distributions of the Fourier transform of 2D pure array $Au_{7\times7}$ at resonance energies (a) 6.49 eV, (b) 8.30 eV, (c) 8.59 eV, and (d) 9.04 eV, and ones of 2D doped array $Au_{7\times7}$-Ni(4,4) at resonance energies (e) 6.44 eV, (f) 8.54 eV, (g) 8.98 eV, and (h) 9.23 eV. (a1) and (a2) correspond to the range $(0,1)$ and $(1,\infty)$, respectively. The integral ranges of (b)–(h) are the same as the above-mentioned ones of (a). Without the effect of $5d$ valence electrons the resonance energies of 2D pure array $Au_{7\times7}$ are (i) 8.03 eV, (j) 8.15 eV, (k) 9.26 eV, and (l) 9.44 eV, respectively. (i)–(l) correspond to the range $(0,\infty)$. The impulse excitation is perpendicular to the planes along the z axis.

inner induced charge, and $6s$ electrons dominate the outer induced charge. In order to get a better understanding of the transversely induced charge distributions of the square arrays, and to observe the clear oscillation mode of s electrons (the s electron plays a major role in the oscillation mode for Au), here we take the integral of the induced charges along the z axis in the range $(-\infty, -1)$, $(-1, 0)$, $(0,1)$, and $(1,\infty)$, respectively, but only show the positive parts (the induced charge distributions are antisymmetric along the z axis). The main peaks correspond to resonance energies 6.49, 8.30, 8.59, and 9.04 eV in the pure square array $Au_{7\times7}$, which are compared with resonance energies 6.44, 8.54, 8.98, and 9.23 eV in the doped square array $Au_{7\times7}$-Ni(4,4), respectively. Both in the doped and pure square arrays, the induced charge distributions are symmetrical in the xy plane. The dopant Ni changes all the induced charge distributions, especially in the region around the doped site, e.g., at a resonance energy 8.54 eV the oscillation of the induced charge in this region is much stronger than the others, as shown in Fig. 13(f1). Away from the doped site, we observe that the oscillation strength of the induced charge in the corner sites experiences small changes by comparing Figs. 13(e1) with 13(a1). This change is more obvious in the range $(1,\infty)$. The charge retains strong oscillation in the four corners of Fig. 13(e2), while it is weak in the corners of Fig. 13(a2). However, the plasmon mode in which the oscillating charge is localized around the Ni atom is not found in both the s- and d-electron regions, and this means that for the out-of-plane plasmons the localized mode still does not exist. In addition, we do not find the obvious features of the TE and TC modes in the pure and doped square arrays. Meanwhile, in Figs. 13(i)–13(l) we also present the induced charge distributions of plasmon resonance in a pure gold square array $Au_{7\times7}$ without $5d$ valence elec-

trons, where the range of the integral of induced charges is $(0,\infty)$. Here, two types of modes, which are similar to TE and TC modes in atomic chains, can be observed very clearly. The two modes correspond to the charge distributions at resonance energies 8.03 and 8.15 eV and 9.26 and 9.44 eV, respectively. In Figs. 13(i) and 13(j) the collective oscillations appear on the four edges of the array, while in Figs. 13(k) and 13(l) the collective oscillations are observed in the wide central area, and we call them the edge mode and center mode, respectively. These plasmons are a bit similar to the transverse modes in Ref. [17]. Therefore, this indicates that the disappearance of the edged and the central characteristics of the transverse modes are caused by an increase in s-d screening and s-d coupling in the 2D array structures.

IV. CONCLUSIONS

Based on the TDDFT calculations, we have systematically compared the electronic excitations of pure gold nanostructures with doped gold nanostructures. The primary conclusions to be drawn from the present work are as follows:

(1) The doped gold chains with a dopant Ni may produce impurity peaks in longitudinal resonance, and the impurity redistributes the corresponding oscillations of induced charge. In the impurity states, the dopant Ni prevents the propagation of induced charge oscillation from one side to another, whereas we do not find the local mode in which local electronic resonances surround the dopant atom as reported in the literature.

(2) The low-limit resonance energies in the transverse modes are larger than those in the longitudinal modes for the atomic chain, which is because of the difference of the needed energies coming from the interband and intraband transitions.

The impurity position has less effect on the optical absorption spectra in the transverse direction. The transverse plasmon resonances with the unobvious features of TE and TC modes can be disrupted by the impurity which mainly suppresses the oscillations of $6s$ electrons in half of the doped chain.

(3) The studies of the effect of d valence electrons show that the $5d$ electrons of gold atoms reduce the energies and oscillation strengths of plasmon resonances for both the longitudinal and transverse modes, and cause the end and center features of the induced charge distributions to be invisible in the transverse modes.

(4) In two-dimensional (2D) gold arrays, with the effect of dopant Ni, the plasmon peaks become unsharp, and the number of peaks increases when the impulse excitation is applied in the x direction. The impurity also changes the whole distributions of induced charge, especially around the impurity. However, a local plasmon mode in which the oscillating charge is localized around dopant Ni does not appear in the 2D arrays. When the direction of impulse excitation is perpendicular to the xy plane, the absorption onset is somewhat lower than that of the 1D situations, and the overall spectrum affected by the Ni atom slightly changes. Meanwhile, the local mode is not found in both the s- and d-electronic oscillating regions. The $5d$ electronic screening and the s-d electronic coupling can cause the edge mode and the center mode to disappear completely in the square arrays.

[1] W. L. Barnes, A. Dereux, and T. W. Ebbesen, Nature (London) **424**, 824 (2003).

[2] E. Prodan, C. Radloff, N. J. Halas, and P. Nordlander, Science **302**, 419 (2003).

[3] P. K. Jain, K. S. Lee, I. H. El-Sayed, and M. A. El-Sayed, J. Phys. Chem. B **110**, 7238 (2006).

[4] S. Kim, J. Jin, Y. J. Kim, I. Y. Park, Y. Kim, and S. W. Kim, Nature (London) **453**, 757 (2008).

[5] J. Zheng, C. Zhou, M. Yu, and J. Liu, Nanoscale **4**, 4073 (2012).

[6] L. Yan, F. Wang, and S. Meng, ACS Nano **10**, 5452 (2016).

[7] D. D. Liu, H. Zhang, and X. L. Cheng, J. Appl. Phys. **112**, 053707 (2012).

[8] S. Kummel, K. Andrae, and P. G. Reinhard, Appl. Phys. B **73**, 293 (2001).

[9] N. J. Halas, S. Lal, W. S. Chang, and S. Link, Chem. Rev. **111**, 3913 (2011).

[10] T. Dong, X. Ma, and R. Mittra, Appl. Phys. Lett. **101**, 233111 (2012).

[11] A. O. Govorov and H. Zhang, J. Phys. Chem. C **119**, 6181 (2015).

[12] H. T. Smith, T. E. Karam, L. H. Haber, and K. Lopata, J. Phys. Chem. C **121**, 16932 (2017).

[13] E. Hutter and J. H. Fendler, Adv. Mater. **16**, 1685 (2004).

[14] S. Gao and Z. Yuan, Phys. Rev. B **72**, 121406(R) (2005).

[15] E. H. Hwang and S. Das Sarma, Phys. Rev. B **75**, 205418 (2007).

[16] J. M. McMahon, S. K. Gray, and G. C. Schatz, Phys. Rev. Lett. **103**, 097403 (2009).

[17] B. J. Wang, Y. Xu, and S. H. Ke, J. Chem. Phys. **137**, 054101 (2012).

[18] E. B. Guidez and C. M. Aikens, Nanoscale **4**, 4190 (2012).

[19] E. B. Guidez and C. M. Aikens, Nanoscale **6**, 11512 (2014).

[20] H. J. Xue, D. P. Hao, M. Zhang, and X. M. Wang, Physica E **86**, 292 (2017).

[21] Y. Wang and Y. B. Yu, Int. J. Mod. Phys. B **31**, 1750233 (2017).

[22] J. Chen, X. L. Cheng, and H. Zhang, Plasmonics **14**, 109 (2019).

[23] R. L. Wu, J. Quan, and M. Sun, Sci. Rep. **8**, 12563 (2018).

[24] L. Yan, M. Guan, and S. Meng, Nanoscale **10**, 8600 (2018).

[25] J. Lin and S. Ke, IOP Conf. Ser.: Mater. Sci. Eng. **562**, 012073 (2019).

[26] H. J. Xue, R. L. Wu, C. X. Hu, and M. Zhang, Int. J. Mod. Phys. B **32**, 1850139 (2018).

[27] J. M. Luther, P. K. Jain, T. Ewers, and A. P. Alivisatos, Nat. Mater. **10**, 361 (2011).

[28] X. Q. Shu, H. Zhang, X. L. Cheng, and Y. Miyamoto, Phys. Rev. B **93**, 195424 (2016).

[29] X. Shu, X. Cheng, and H. Zhang, Phys. Chem. Chem. Phys. **20**, 10439 (2018).

[30] K. M. Conley, N. Nayyar, T. P. Rossi, M. Kuisma, V. Turkowski, M. J. Puska, and T. S. Rahman, ACS Nano **13**, 5344 (2019).

[31] M. H. Khodabandeh, N. Asadi-Aghbolaghi, and Z. Jamshidi, J. Phys. Chem. C **123**, 9331 (2019).

[32] B. Gao, K. Ruud, and Y. Luo, J. Chem. Phys. **137**, 194307 (2012).

[33] J. Yan, Z. Yuan, and S. Gao, Phys. Rev. Lett. **98**, 216602 (2007).

[34] J. Yan and S. Gao, Phys. Rev. B **78**, 235413 (2008).

[35] G. Piccini, R. W. A. Havenith, R. Broer, and M. Stener, J. Phys. Chem. C **117**, 17196 (2013).

[36] F. Ding, E. B. Guidez, C. M. Aikens, and X. Li, J. Chem. Phys. **140**, 244705 (2014).

[37] R. D. Senanayake, D. B. Lingerfelt, G. U. Kuda-Singappulige, X. Li, and C. M. Aikens, J. Phys. Chem. C **123**, 14734 (2019).

[38] J. Tersoff and D. R. Hamann, Phys. Rev. B **31**, 805 (1985).

[39] G. Binnig, C. F. Quate, and C. Gerber, Phys. Rev. Lett. **56**, 930 (1986).

[40] P. Dawson, F. de Fornel, and J. P. Goudonnet, Phys. Rev. Lett. **72**, 2927 (1994).

[41] Y. K. Kim and J. B. Ketterson, Opt. Lett. **21**, 165 (1996).

[42] N. Nayyar, V. Turkowski, and T. S. Rahman, Phys. Rev. Lett. **109**, 157404 (2012).

[43] M. A. L. Marques, A. Castro, G. F. Bertsch, and A. Rubio, Comput. Phys. Commun. **151**, 60 (2003).

[44] A. Castro, H. Appel, M. Oliveira, C. A. Rozzi, X. Andrade, F. Lorenzen, M. A. L. Marques, E. K. U. Gross, and A. Rubio, Phys. Status Solidi B **243**, 2465 (2006).

[45] P. A. M. Dirac, Math. Proc. Cambridge Philosophical Soc. **26**, 376 (1930).

[46] J. P. Perdew and A. Zunger, Phys. Rev. B **23**, 5048 (1981).

[47] C. Hartwigsen, S. Goedecker, and J. Hutter, Phys. Rev. B **58**, 3641 (1998).

[48] T. Lu and F. Chen, J. Comput. Chem. **33**, 580 (2012).

[49] N. Nilius, T. M. Wallis, and W. Ho, Science **297**, 1853 (2002).

[50] K. Y. Lian, P. Salek, M. Jin, and D. Ding, J. Chem. Phys. **130**, 174701 (2009).

[51] W. Li and F. Chen, Appl. Phys. A: Mater. Sci. Process. **113**, 543 (2013).

[52] J. P. Perdew, J. A. Chevary, S. H. Vosko, K. A. Jackson, M. R. Pederson, D. J. Singh, and C. Fiolhais, Phys. Rev. B **46**, 6671 (1992).

[53] J. P. Perdew, J. A. Chevary, S. H. Vosko, K. A. Jackson, M. R. Pederson, D. J. Singh, and C. Fiolhais, Phys. Rev. B **48**, 4978 (1993).

[54] J. P. Perdew, K. Burke, and M. Ernzerhof, Phys. Rev. Lett. **77**, 3865 (1996).

[55] R. Armiento and A. E. Mattsson, Phys. Rev. B **72**, 085108 (2005).

[56] A. E. Mattsson, R. Armiento, J. Paier, G. Kresse, J. M. Wills, and T. R. Mattsson, J. Chem. Phys. **128**, 084714 (2008).

[57] A. D. Becke, J. Chem. Phys. **98**, 5648 (1993).

[58] K. Yabana and G. F. Bertsch, Phys. Rev. A **60**, 3809 (1999).

[59] J. C. Idrobo, S. Ogut, and J. Jellinek, Phys. Rev. B **72**, 085445 (2005).

[60] D. D. Liu and H. Zhang, Chin. Phys. B **20**, 097105 (2011).

[61] B. J. Wang and S. H. Ke, Integr. Ferroelectr. **146**, 105 (2013).

[62] A. Liebsch, Phys. Rev. Lett. **71**, 145 (1993).